Applied Catalysis B: Environmental 180 (2016) 344–350

Contents lists available at ScienceDirect

Applied Catalysis B: Environmental

journal homepage: www.elsevier.com/locate/apcatb

Preparation of hollow Ag/Pt heterostructures on TiO_2 nanowires and their catalytic properties

Liangshu Jiang [a], Wenhao Zhu [a], Chaoyang Wang [a], Wenjun Dong [a,b,*], Longfei Zhang [a], Ge Wang [b,*], Benyong Chen [a], Chaorong Li [a], Xiaobo Zhang [a]

[a] Center for Nanoscience and Nanotechnology, Zhejiang Sci-Tech University, Hangzhou 310018, China
[b] Beijing Key Laboratory of Function Materials for Molecule & Structure Construction, School of Materials Science and Engineering, University of Science and Technology Beijing, Beijing 100083, PR China

ARTICLE INFO

Article history:
Received 30 March 2015
Received in revised form 12 June 2015
Accepted 17 June 2015
Available online 23 June 2015

Keywords:
Ag/Pt
Heterostructure
Hollow
Interfaces
Catalytic property

ABSTRACT

A novel titanate (TiO_2) nanowire (NW)@hollow silver (Ag)/platinum (Pt) heterostructure was fabricated by means of a simple wet chemical method. Briefly, Ag nanoparticles with ~20 nm in diameter were grown onto TiO_2 nanowires, subsequently PtO shells with ~1 to 4 nm in thickness were deposited upon the Ag nanoparticles to form TiO_2–NW@Ag–NP@PtO nanostructures. The hollow Ag-/PtO_x nanostructures were achieved from Ag–NP@PtO nanostructures by outward diffusion of Ag elements from Ag–NP core to PtO shell *via* H_2O_2 treatment. Finally, hollow Ag/Pt heterostructures with diameter of approximately 20 nm were synthesized by reduction of the hollow Ag-/PtO_x nanostructures. Given the accessible interfaces of bimetallic Ag/Pt shell, the catalytic efficiency of the TiO_2 NW@hollow Ag/Pt heterostructures was significantly enhanced, which was confirmed by the hydrogenation of *p*-nitrophenol into *p*-aminophenol with $NaBH_4$ as reducing agent in aqueous phase. The conversion rate of *p*-nitrophenol was yielded as high as ~95% for 9 min under ambient atmosphere and room temperature.

1. Introduction

Multimetallic nanostructures [1], in particular bimetallic nanostructures, have attracted considerable interest owing to their remarkable electronic [2], optical [3], and catalytic [4] properties. Of these, the complex bimetallic heteronanostructures with diverse morphologies, such as core–shell nanoparticles [5,6], hollow nanospheres [7–10] and yolk-shell nanostructures [11,12], exhibit outstanding catalytic properties.

To date, a variety of bimetallic nanostructures have been fabricated for catalytic applications [13]. Ag-doped Pt nanoparticle catalysts were synthesized to perform high hydrogen activation in transformation C_2H_2 to C_2H_4 at high reaction temperatures, by utilizing their inherent phase-segregation-function to provide preferential access to chemically selective C_2H_2 hydrogenation sites [14,15]. Concave Au@Pt nanocubes with a unique plasmonic optical property exhibit an improved catalytic activity, which is attributed to the large surface area, rich atomic steps and the synergistic effect between Au and Pt [16]. Recent research work also confirms that the introduction of bimetallic interfaces, such as bimetallic hollow structures, improves the catalytic performance of metal catalysts to a great magnitude, and increases the surface area and the utilization efficiency of new metal catalysts [17]. Particularly, the bimetallic interface between Ag and Pt with different work functions facilitates an electron relay system, which opens up a pathway for diverse intermediate steps in the reaction of adsorbed species and enhancement in the activity of Pt/Ag catalysts [18]. Similarly, bimetallic hollow nanostructures greatly enhance the accessible interface, which also improves the electron transfer property for high catalytic activity. For example, Co-Pt hollow spheres exhibit a unique electrocatalytic activity toward methanol oxidation in comparison with ordinary Co-Pt nanoparticle counterparts [19]. Hollow Pt-Ni nanospheres with electron-deficient Pt active sites can enhance the catalytic activity of liquid-phase *p*-chloronitrobenzene hydrogenation to *p*-chloroaniline [20]. However, the synthesis of hollow hetero-nanostructures with bimetallic interfaces and various work functions to improve the catalytic activity and accessible interfaces remain a challenge.

* Corresponding authors at: Center for Nanoscience and Nanotechnology, Zhejiang Sci-Tech University, Hangzhou 310018, China. Fax: +86 010 62333827.
E-mail addresses: wdong@ustb.edu.cn (W. Dong), gewang@mater.ustb.edu.cn (G. Wang).

http://dx.doi.org/10.1016/j.apcatb.2015.06.033
0926-3373/

In this work, TiO_2 NW@hollow Ag/Pt heterostructures were synthesized to perform a desirable catalytic function. In a typical preparative process, Ag nanoparticles were grown on TiO_2 nanowires, followed by the deposition of PtO shells on the Ag–TiO_2 system to form TiO_2 NW@Ag–NP@PtO nanostructures. Subsequently, hollow feature of the Ag-/PtO_x nanostructures were realized by outward diffusion of Ag elements from Ag–NP core to PtO_x shell. Finally, hollow Ag/Pt heterostructures were obtained by the reduction of the hollow Ag-/PtO_x nanostructures. Interestingly, the step by step reaction avoids the formation of Ag/Pt alloy structure, and the catalytic efficiency of the hollow Ag/Pt heterostructures is greatly enhanced due to the bimetallic and accessible interface between Ag and Pt. Furthermore, TiO_2 nanowires, as a catalyst support, can eliminate the aggregation of active Ag/Pt particles and realize essential reusability of the catalyst. The TiO_2NW@hollow Ag/Pt heterostructures with numerous accessible interfaces of metallic components demonstrate an excellent catalytic performance to hydrogenate *p*-nitrophenol with $NaBH_4$ as reducing agent in aqueous phase.

2. Experimental

2.1. Reagents

$AgNO_3$, K_2PtCl_4, NaOH, $NH_3{\cdot}H_2O$, ethanol, H_2O_2 and trisodium citrate were purchased from Sigma–Aldrich, and all the reagents were used without further purification. TiO_2 nanowires were synthesized according to the previously reported method [21].

2.2. Preparation of TiO_2 NW@Ag–NP@PtO nanostructures

TiO_2 NW@Ag-NP@PtO nanostructures were prepared by a solution reaction. Firstly, TiO_2 nanowires were added to a mixed solution containing 20 mL absolute ethanol and 20 mL $Ag(NH_3)_2NO_3$ (0.10 mol/L) solution under vigorous magnetic stirring at room temperature, and the mixture was further stirred for 30 min at 70 °C. TiO_2 NW@Ag NP nanostructures were obtained by filtration, rinsed with deionized water and dried at 70 °C for 5 h. Subsequently, 20 mL K_2PtCl_4 aqueous solution was refluxed with stirring at 110 °C for 60 min in oil bath. Afterwards, the TiO_2 NW@Ag NP nanostructures were added into K_2PtCl_4 solution and stirred for 10 min. Finally, 80 μL aqueous trisodium citrate solution (38.8 m mol/L) was added to this solution quickly. The mixture was refluxed for 60 min to obtain the TiO_2 NW@Ag–NP@PtO nanostructures, and then naturally cool down to room temperature. TiO_2 NW@Ag–NP@PtO nanostructures were collected and rinsed with deionized water.

2.3. Preparation of TiO_2 NW@hollow Ag/Pt heterostructures

TiO_2 NW@Ag–NP@PtO nanostructures were added into 10 mL H_2O_2 solution (15 wt%) and stirred for a few minutes, and then TiO_2 NW@hollow Ag/PtO_x nanostructures were obtained. Finally, the TiO_2 NW@hollow Ag/PtO_x nanostructures were added into 10 mL aqueous $NaBH_4$ solution (0.10 mol/L). TiO_2 NW@hollow Ag/Pt heterostructures were collected, rinsed with deionized water and dried in air.

2.4. Characterizations and catalytic activities of the yielded products

Morphology and size of the products were characterized using JEOL JEM 2010 transmission electron microscopy (TEM), equipped with energy-dispersive X-ray spectroscopy (EDX) for determination of chemical composition. The samples for TEM measurements were prepared by dispersing the suspension containing target samples in distilled water and dried on a porous carbon film. X-ray photoelectron spectroscopy (XPS, VGESCALABMKII) was used for elemental analysis using non-monochromatized Al-Kα X-ray ($h\gamma = 1486.6$ eV) as excitation source. The obtained binding energies were corrected by referencing the C1s to 284.7 eV.

To study the catalytic activity of the synthesized products, a freshly prepared aqueous solution of $NaBH_4$ (1.00 mL, 0.1 mol/L) was added into 50.0 mL of *p*-nitrophenol aqueous solution (1×10^{-4} mol/L) under constant stirring at room temperature. Later, 1.5 mg of each catalyst (*i.e.* TiO_2 NW@hollow Ag-/PtOx, TiO_2 NW@Ag–NP@PtO, TiO_2 NW@Ag NP and TiO_2 NW@Pt NP) was added in the above mixture, respectively. Moreover, excessive NaBH4 in the mixture can quickly reduce the TiO_2 NW@hollow Ag-/PtO_x catalysts (TiO_2 NW@Ag–NP@PtO catalysts) to TiO_2 NW@hollow Ag/Pt catalysts (TiO_2 NW@Ag NP@Pt catalysts) with 100% yield rate. The mixture was collected at an interval of reaction time, and UV–vis absorption spectra were recorded to monitor the reaction (Hitachi U-3900 UV–vis spectrophotometer). The catalysts were collected, rinsed with deionized water, and dried in vacuum for 12 h for the next catalysis run under identical conditions.

3. Results and discussion

3.1. Structural and morphological characterization

TEM image (Fig. 1a) of the TiO_2 NW@Ag NP nanostructures, synthesized by mixing TiO_2 NW and $Ag(NH_3)_2NO_3$ in ethanol aqueous solution at 70 °C for 30 min, illustrates the Ag nanoparticles, with a diameter of 10∼30 nm, were orderly grown onto TiO_2 nanowires (inset in Fig. 1a). EDX analysis confirms that only Ti, Ag and O elements were present in the TiO_2 NW@Ag NP nanostructures, indicating that the Ag nanoparticles were modified on TiO_2 NW (Fig. 1b). When PtO layers were subsequently deposited onto the individual Ag nanoparticles on the surface of the TiO_2 NW, TiO_2 NW@Ag–NP@PtO nanostructures were obtained (Fig. 1c). However, Ag–NP was transferred into Ag/AgCl composites due to low stability of Ag nanoparticles at 110 °C. TEM image of the TiO_2 NW@Ag–NP@PtO nanostructures (inset in Fig. 1c) reveals that the PtO layers of about 2 nm in thickness covered the Ag–NP. EDX spectrum of TiO_2 NW@Ag–NP@PtO nanostructures, suggesting that the PtO layers were deposited on Ag cores (Fig. 1d). However, the low stability of Ag–NP@PtO nanostructures when being exposed to 200 kV electron beam irradiation inside TEM chamber, and the decomposition of AgCl into Ag nanoparticles [22], led to the formation of Ag@PtO yolk–shell nanostructures (inset in Fig. 1c), which is similar to the previous study [23]. When the Ag–NP@PtO nanostructures were immersed into H_2O_2 aqueous solution, Ag began immigrating from Ag–NP core (Ag/AgCl composites) toward PtO shell, and hollow Ag-/PtO_x nanostructures were obtained within 7 min. Finally, uniform hollow Ag/Pt heterostructures modified on TiO_2 NW (Fig. 1e) were synthesized by reduction of Ag-/PtO_x into Ag/Pt with the aid of $NaBH_4$, and the SEM and TEM images with larger area were provided as follows (SI Fig. S1). TEM image of the TiO_2 NW@hollow Ag/Pt heterostructures unveils that hollow Ag/Pt heterostructures were about 20 nm in diameter and 5 nm in thickness (inset in Fig. 1e). The TiO_2 NW@hollow Ag/Pt heterostructures contain Ti, Ag, Pt and O (Fig. 1f).

3.2. Chemical composition analysis

Chemical state of Pt plays an important role in performing its catalytic activity [24,25]. As such, XPS was employed to determine

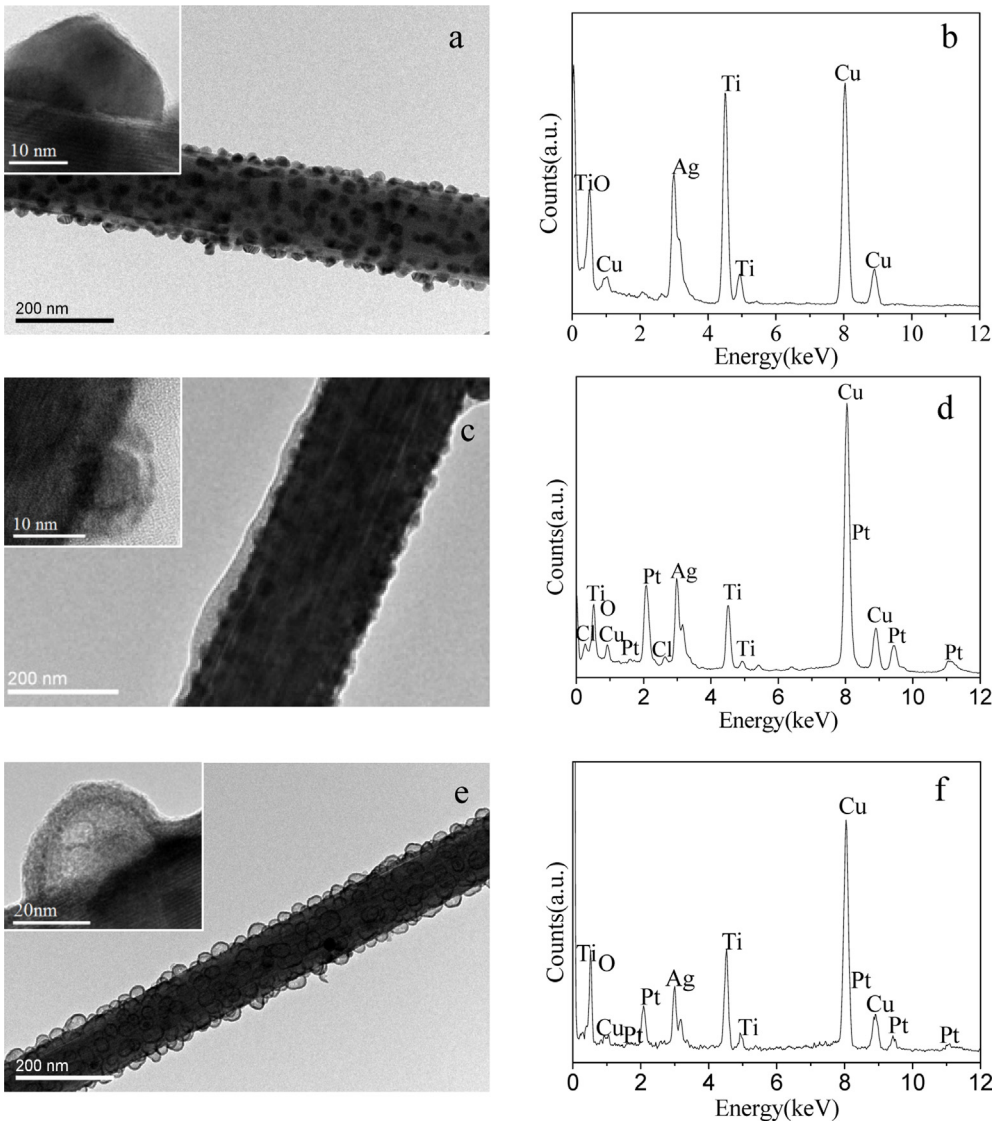

Fig. 1. Representative TEM images and EDX spectra of (a, b) TiO_2 NW@Ag NP nanostructures, (c, d) TiO_2 NW@Ag–NP@PtO nanostructures and (e, f) TiO_2 NW@hollow Ag/Pt heterostructures.

the chemical state of the synthesized products, and to elucidate the catalytic performance. The survey spectra (SI Fig. S2) conform the presence of Pt, Ag, Ti, O elements. XPS spectra of Pt (4f) in the products (TiO_2 NW@Ag–NP@PtO, TiO_2 NW@hollow Ag-/PtO_x and TiO_2 NW@hollow Ag/Pt) are depicted in Fig. 2a. A peak shift of 2.0 eV of Pt $4f_{7/2}$ from the lower (72.8 eV) to the higher (74.8 eV) binding energy clearly indicates that oxidization of Pt^{2+} into Pt^{4+} took place during the immersion of TiO_2 NW@Ag–NP@PtO nanostructures in H_2O_2 aqueous solution. Regarding to TiO_2 NW@hollow Ag-/PtO_x catalyst, Pt($4f_{7/2}$) peaks at 72.8 and 74.8 eV can be attributed to Pt^{2+}(PtO) and Pt^{4+}(PtO_2), respectively [26,27]. Moreover, majority of Pt presents as Pt^{4+}. XPS spectra of Pt in the TiO_2 NW@hollow Ag/Pt catalyst demonstrate that the PtO_x was reduced to Pt^0 by $NaBH_4$. XPS spectrum of Ag in the TiO_2 NW@Ag–NP@PtO shows that Ag was dispersed in Ag^+ and Ag^0 (Fig. 2b) [22], which is in agreement with the XRD results (SI Fig. S3). A slight shift of the Ag $3d_{5/2}$ binding energy in the TiO_2 NW@hollow Ag-/PtO_x catalyst from that of the TiO_2 NW@Ag–NP@PtO catalyst suggests that an oxidizing reaction occurred, transforming Ag^0 (Ag–NP) into Ag^+. Furthermore, the XPS spectrum of Ag in the TiO_2 NW@hollow Ag/Pt catalyst indicates that Ag^+ was reduced to Ag^0 by $NaBH_4$.

3.3. Formation mechanism of TiO_2 NW@hollow Ag/Pt heterostructures

The formation process of TiO_2 NW@hollow Ag/Pt heterostructures was illustrated in Scheme 1. At the initial stage, Ag nanoparticles with approximately 20 nm in diameter were grown onto TiO_2 NW, and followed by the deposition of PtO shells with ~1 to 4 nm in thickness upon the Ag nanoparticles to yield TiO_2NW@Ag–NP@PtO nanostructures. When the Ag–NP@PtO nanostructures were exposed to H_2O_2 solution, the dominant chemical potential difference between Pt and Ag drove the occurrence of outward diffusion of Ag elements from Ag–NP core toward PtO_x shell. Given such diffusion effect of Ag, internal Ag core diffused outwards until approaching boundary sites and enlarging voids, and the nucleation and growth of hollow Ag-/PtO_x nanostructures occurred on the surface of PtO_x nanostructures. Furthermore, the dissolution of Ag core increased the concentrations of Cl^- on the locations of etched Ag, leading to the growth of pits by autocatalytic processes [28]. As a result, TiO_2 NW@hollow Ag-/PtO_x nanostructures were generated. Finally, TiO_2 NW@hollow Ag-/PtO_x nanostructures were reduced by $NaBH_4$ to form TiO_2 NW@hollow Ag/Pt heterostructures with the accessible interface between Ag

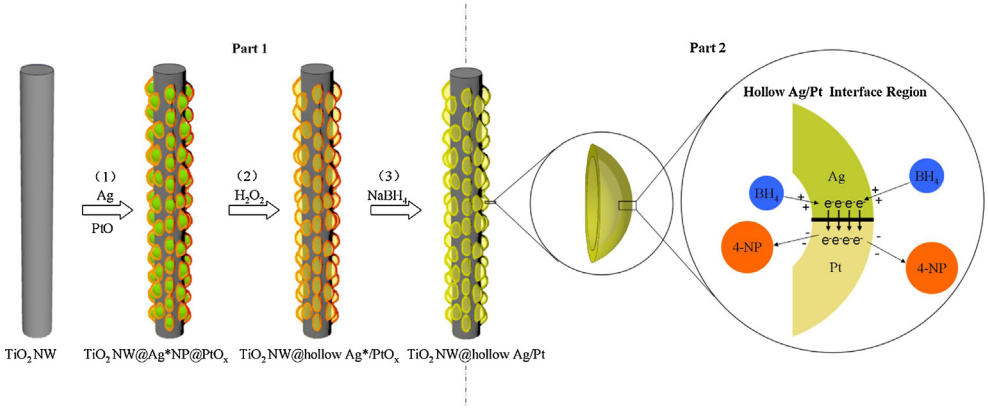

Scheme 1. Schematic illustration of the formation mechanism of TiO_2 NW@hollow Ag/Pt heterostructures.

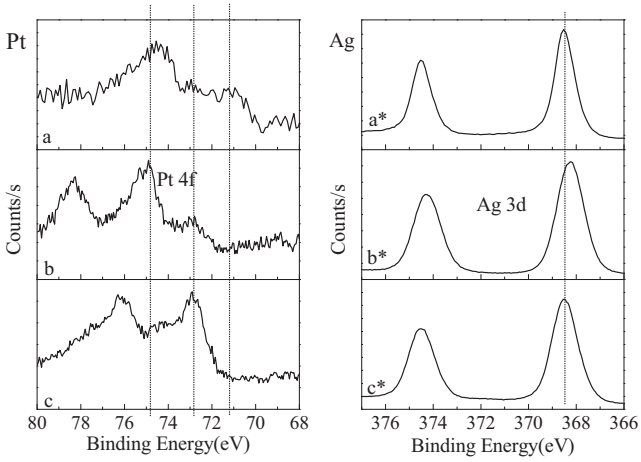

Fig. 2. XPS spectra of Pt4f and Ag3d regions for TiO_2 NW@hollow Ag/Pt heterostructures (a, a*), TiO_2 NW@hollowAg-/PtO_x nanostructures (b, b*) and TiO_2 NW@Ag–NP@PtO nanostructures (c, c*).

and Pt. The presence of such interface between two dissimilar metals with different work functions contributes greatly to enhanced the catalytic activity of the bimetallic hollow Ag/Pt nanostructures in two perspectives: (1) providing the accessible interfaces and high surface-to-volume ratio; (2) supplying defects, vacancies and boundaries incurred by the outward diffusion of Ag element from Ag–NP core toward PtO shell [29,30].

3.3.1. Reaction of TiO_2 NW@Ag–NP@PtO nanostructures with H_2O_2

The reaction of TiO_2 NW@Ag–NP@PtO nanostructures with H_2O_2 results in TiO_2 NW@hollow Ag-/PtO_x nanostructures. H_2O_2 plays a vital role in diffusing Ag element from Ag–NP core to PtO shell [31]. Ag–NP core was oxidized by H_2O_2 under acidic condition as indicated by the following reaction:

$$\text{Ag-NP} + H_2O_2 + H^+ \rightarrow Ag^+ + H_2O \quad (1)$$

On the other hand, the produced Ag^+ diffused from Ag–NP core to PtO_x shell, and subsequently Ag^+ was reduced by H_2O_2 to ultrafine Ag nanoparticles on the shell. The reaction of Ag^+ with H_2O_2 was confirmed by the continuous bubbles produced in the solution.

$$Ag^+ + H_2O_2 + \text{PtOshell} \rightarrow \text{Ag-/PtO}_x\text{shell} + O_2\uparrow + H^+ \quad (2)$$

Meanwhile, the PtO shells of the TiO_2 NW@Ag–NP@PtO nanostructures were *in situ* oxidized to PtO_x (PtO_2 and PtO) in the Ag-/PtO_x shell by H_2O_2. Recent studies also report that the Pt-oxide prevents the dissolution of Pt in the presence of H_2O_2 and H_2O_2 facilitates *in situ* oxidation of PtO to PtO_2 [32].

3.4. Catalytic activities

Catalytic activities of the synthesized products in terms of reduction of *p*-nitrophenol into *p*-aminophenol with aid of $NaBH_4$ were investigated, and the conversion process was monitored by UV–vis absorption spectroscopy. In the catalytic reaction, an excessive quantity of $NaBH_4$ was employed to perform three purposes: (i) reducing AgCl/PtO_x into Ag/Pt within the catalysts; (ii) protecting the *p*-aminophenol from aerial oxidation; and (iii) controlling independent reduction rate regardless the concentration of $NaBH_4$ [33–35]. Moreover, excessive $NaBH_4$ can reduce the TiO_2 NW@hollow Ag-/PtO_x catalysts (TiO_2 NW@Ag–NP@PtO catalysts) to TiO_2 NW@hollow Ag/Pt catalysts (TiO_2 NW@Ag NP@Pt catalysts) with 100% yield rate within 5 s.

The reducing reaction of *p*-nitrophenol into *p*-aminophenol can be summarized by the following equation:

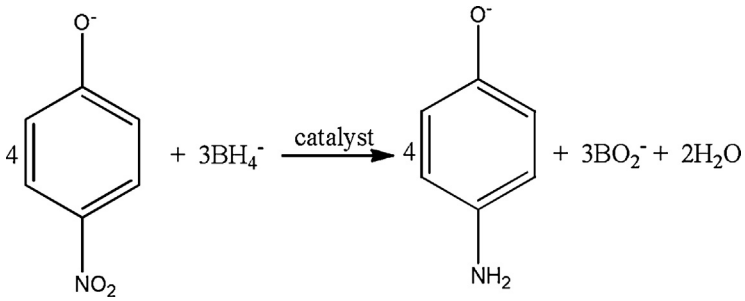

(3)

The reaction of *p*-nitrophenol with $NaBH_4$ is a thermodynamically favorable process. The electrochemical potential of *p*-nitrophenol/*p*-aminophenol is −0.76 V_{SCE} and the electrochem-

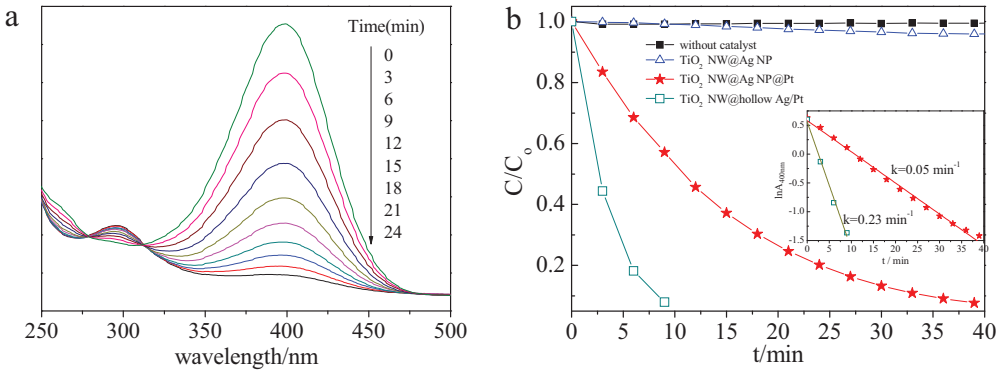

Fig. 3. (a) Successive UV–vis absorption spectra of the reduction of *p*-nitrophenol by $NaBH_4$ in the presence of the TiO_2 NW@hollow Ag/Pt catalyst at different reaction times, indicating the decrease in the intensity for the peak at 400 nm associated with *p*-nitrophenol as the reduction of the —NO_2 group to an —NH_2 group. (b) C_t/C_0 *versus* reaction time for the reduction of *p*-nitrophenol, no catalyst, TiO_2 NW@Ag NP, TiO_2 NW@ Ag/Pt NP, and TiO_2 NW@hollow Ag/Pt nanostructure catalysts, and the k_{app} of TiO_2 NW@Ag NP@Pt and the TiO_2 NW@hollow Ag/Pt catalyst (the inset in Fig. 3b).

ical potential of H_3BO_3/BH_4^- is −1.33 V_{SCE}. However, such a reduction is a kinetically restricted reaction (initiated 2 days later) without the catalyst tested. The absorption spectrum of the aqueous mixture of *p*-nitrophenol and $NaBH_4$ exhibits a peak at 400 nm that is a characteristic peak of the *p*-nitrophenolate ions. When the catalyst was added into the mixture of *p*-nitrophenol and $NaBH_4$, the absorbance peak at shifts from 400 nm down to 300 nm, corresponding to *p*-aminophenol, suggesting the reduction product of *p*-nitrophenol. Fig. 3a depicts the UV–vis absorption spectra of the *p*-nitrophenol reduction by $NaBH_4$ in the presence of catalyst. The reduction followed a pseudo-first-order reaction due to the presence of excessive $NaBH_4$. The values of the rate constants (k_{app}) of the catalytic reactions were estimated from the plot of $\ln A_{400nm}$ (A_{400nm} is the absorbance at 400 nm) *versus* time. Fig. 3b shows the C/C_0 (C_0 is the initial concentration of *p*-nitrophenol and C is the concentration of *p*-nitrophenolate as a function of time, t) and lnA *versus* reaction time for the reduction of *p*-nitrophenol in the presence of the respective TiO_2 NW@Ag NP, TiO_2 NW@Ag NP@Pt and TiO_2 NW@hollow Ag/Pt catalysts. Apparently, when the TiO_2 NW@Ag NP catalyst was added into the aqueous mixture of *p*-nitrophenol and $NaBH_4$, the reaction was finalized by 120 min. When the TiO_2 NW@Ag NP@Pt catalyst was involved, the reaction duration was shortened into 40 min. The k_{app} of TiO_2 NW@Ag NP@Pt catalyst was 0.05 min^{-1} (inset in Fig. 3b). When TiO_2 NW@hollow Ag/Pt catalyst (k_{app} = 0.23 min^{-1}) was utilized, the reaction was completed within 9 min. The catalytic efficiency of TiO_2 NW@hollow Ag/Pt heterostructures was enhanced due to a larger accessible interface and higher aspect (surface-to-volume) ratio.

Fig. 4a shows the plot of $\ln(C/C_0)$ of TiO_2 NW@hollow Ag/Pt catalysts as a function of time measured at various temperatures. The values of k at various temperatures (25, 37 and 52 °C) were estimated from the slope of the linear part of the plots, and the activation energy was determined accordingly. Fig. 4b depicts the linear fitting of lnk as a fucniton of 1/T, and the apparent activation energy (E_a) can be calculated from the Arrhenius equation:

$$\ln k = \ln A - E_a/RT$$

The calculated E_a value is approximately 52.4 kJ/mol, where lnA is the intercept of the line and R is the constant of gas.

Reusability is an important property for catalysts. Typically, hollow nanostructured catalysts suffer from both low separation efficiency and easy reduced catalytic activity. The hollow Ag/Pt heterostructures decorated on the TiO_2 NW with good stability and dispersibility were designed to enhance the recycling and reusability of the catalysts. After 3 cycles of catalytic hydrogenation of *p*-nitrophenol using TiO_2 NW@hollow Ag/Pt catalyst, the conversion efficiency remains at 90%, and the TiO_2 NW@hollow Ag/Pt still can maintain the morphology of the as-prepared samples, indicating a good stability and outstanding recyclability of the catalyst (SI Fig. S4). After eight cycles of catalytic hydrogenation, the conversion efficiency of the TiO_2 NW@hollow Ag/Pt catalysts remains at 88%, which is slightly lower than that in the first run (93%), indicating an outstanding recyclability of the catalyst (Fig. 5). It demonstrates that the TiO_2 NW@hollow Ag/Pt catalysts are capable of efficient decomposition of organic contaminants for long-lasting and recycle applications.

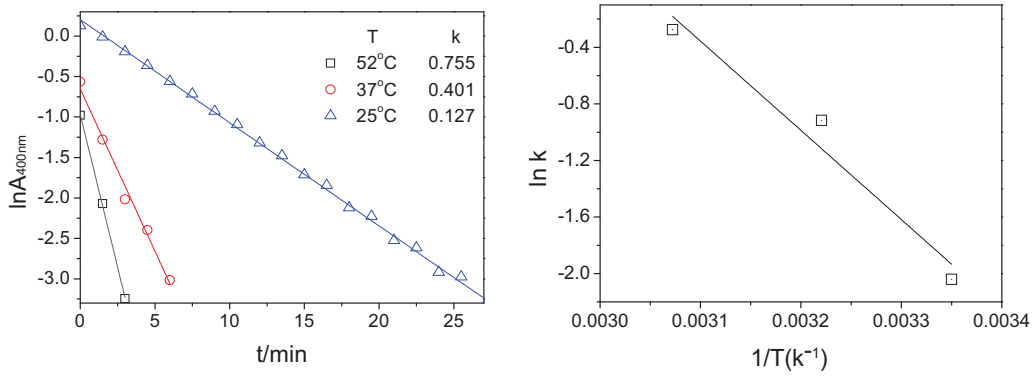

Fig. 4. (a) Plot of time *versus* $\ln A_{400nm}$ by TiO_2 NW@hollow Ag/Pt heterostructures at different temperatures (*p*-nitrophenol:100 mL, $NaBH_4$:2.0 mL, catalyst:1.5 mg); (b) Arrhenius plot of $\ln k_{app}$ *vs* (1/T).

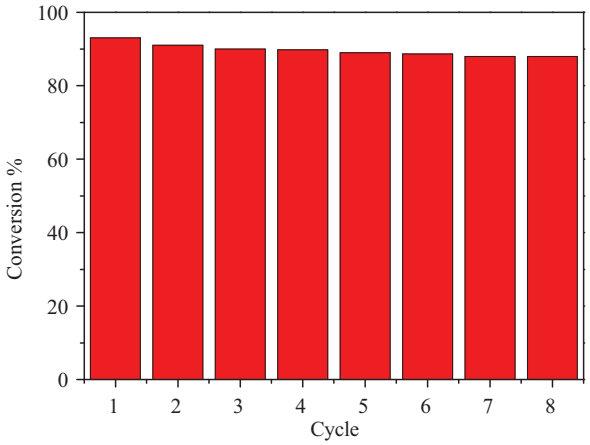

Fig. 5. The correlation of the conversion of *p*-nitrophenol with the number of catalyst recycles.

3.4.1. *Effect of Pt/Ag ratio on the reactivity of the catalysts*

In terms of the TiO_2 NW@Ag NP@Pt nanostructures, Ag NPs were a structural pier for the Pt shell, which can increase the utilization of Pt, and enhance the catalytic performance. Fig. 6a depicts the C/C_0 *versus* reaction time for the reduction of *p*-nitrophenolate in the presence of over TiO_2 NW@Ag NP, TiO_2 NW@Pt NP and TiO_2 NW@Ag NP@Pt catalysts, respectively. Obviously, all the reductions catalyzed by TiO_2 NW@Ag NP@Pt catalyst proceeded faster than those catalyzed by the TiO_2 NW@Ag NP and TiO_2 NW@Pt NP catalyst, indicating that an enhanced catalytic activity derived from its high surface-to-volume ratio and synergistic core/shell effect [36]. The TiO_2 NW@Ag NP@Pt nanostructured catalysts with various Pt shell thicknesses were obtained by changing the quantity of K_2PtCl_4 (SI Fig. S5). In the case of the TiO_2 NW@Ag NP@Pt nanostructured catalyst prepared by using 20 mL 50 μM K_2PtCl_4 solution, the Pt shell thickness is 1 nm. When the amount of the Pt precursor increases up to 100 μM K_2PtCl_4, the Pt shell thickness increases to 2 nm. With a further increase in the amount of Pt precursor (200 μM), the Pt shell thickness goes up to 4 nm. The Pt/Ag molar ratio of the composite is 0.13, 0.39 and 0.68, respectively (Table S1). Results reveal that higher amount of Pt source in the precursor solutions elicits both larger the Pt shell thickness and higher Pt/Ag molar ratio. Fig. 6b presents k_{app} dependence on Pt shell thickness of the TiO_2 NW@Ag NP@Pt catalysts. The TiO_2 NW@Ag NP@Pt catalyst (1 nm) exhibits higher catalytic activity compared with TiO_2 NW@Ag NP@Pt catalyst (2 nm, 4 nm), which indicates that the catalytic efficiency of the TiO_2 NW@Ag NP@Pt catalyst (1 nm) was enhanced due to the Ag nanoparticles exposure and the synergistic effect between Ag and Pt. In order to control the leaching of Ag, the TiO_2 NW@Ag NP@Pt catalyst (2 nm Pt shell) was selected as the precursor to generate TiO_2NW@hollow Ag/Pt catalyst with satisfactory stability.

3.4.2. *Interfacial effect on the reactivity of the catalysts*

It is well known that bimetallic nanostructures can enhance the activity of the catalyst, which is attributed to the presence of distinguished interface between dissimilar metals performing different functions [37]. Fig. 6c and d displays the C/C_0 and lnA *versus* reaction time for the reduction of *p*-nitrophenol over the TiO_2 NW@hollow Ag/Pt catalysts. The rate constant k_{app} of the TiO_2 NW@hollow Ag/Pt catalyst was controlled between 0.12 and 0.23 min^{-1}. TiO_2 NW@hollow Ag/Pt catalysts exhibit a higher activity than TiO_2 NW@Ag NP@Pt (Fig. 6), indicating that more bimetallic interfaces were obtained by dispersing Ag nanoparticles dispersed in Pt shells. The inset image in Fig. 6d exhibits the rate constant k_{app} curve for the reduction of *p*-nitrophenol over TiO_2 NW@hollow Ag/Pt cata-

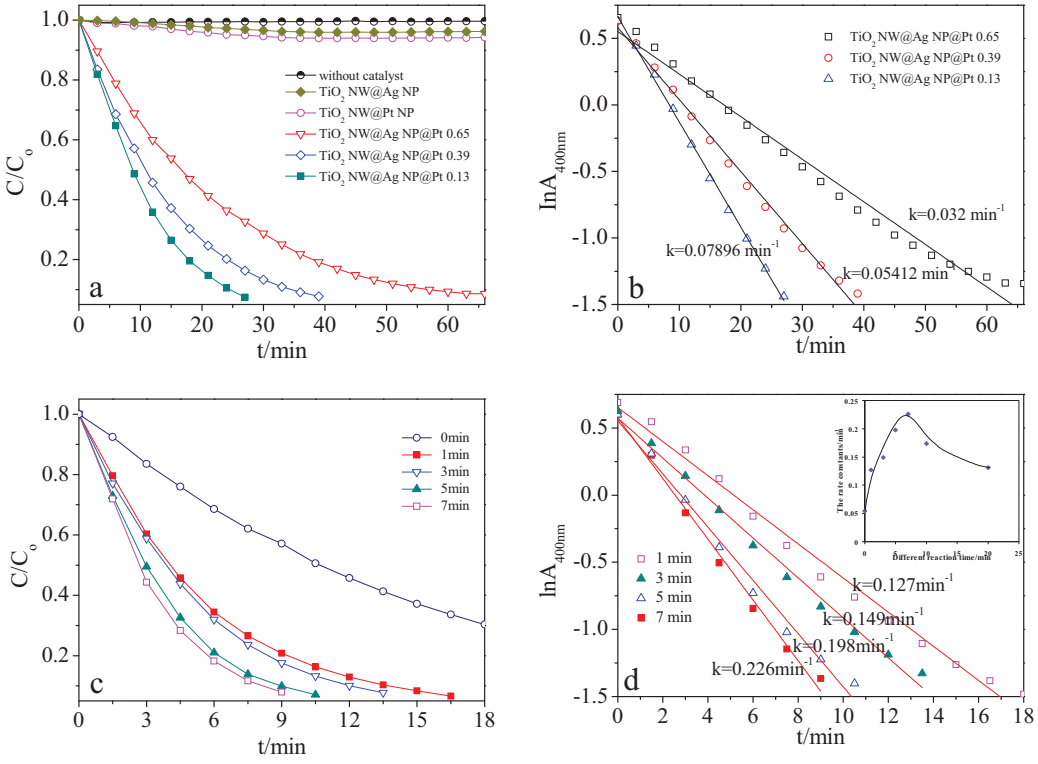

Fig. 6. (a) Extinction at the peak position for *p*-nitrophenol (400 nm) as a function of time with TiO_2 NW@Ag NP@Pt nanostructures; (b) Plot of reduction time *vs* ln(A_{400nm}) by TiO_2 NW@Ag NP@Pt nanostructures; (c) Extinction at the peak position for *p*-nitrophenol (400 nm) as a function of time with TiO_2 NW@hollow Ag/Pt heterostructures used as catalysts; (d) Plot of reduction time *vs* ln(A_{400nm}) by TiO_2 NW@hollow Ag/Pt heterostructures catalysts, and the catalytic rate *vs* reaction time of the TiO_2 NW@Ag NP@PtO and H_2O_2 aqueous (the inset in Fig. 6d).

lysts. When short reaction time (TiO_2 NW@Ag NP@PtO catalysts and H_2O_2 aqueous) was applied (less than 7 min), the catalytic rate increased with reaction time, indicating that the dispersibility of ultrafine Ag nanoparticles in Pt shells was increased and numerous accessible interfaces between Ag and Pt were obtained. However, when reaction time exceeded 7 min, the catalytic rate was decreased with reaction time due to the less accessible bimetal interfaces and the reduced Pt sites (SI Fig. S6). Moreover, the constant molar ratio of Pt/Ag in the TiO_2 NW@hollow Ag/Pt heterostructures catalysts confirms a good stability of the catalyst. The TiO_2 NW@hollow Ag/Pt catalyst (7 min) exhibited higher catalytic activity due to accessible bimetallic interfaces obtained by the superfine Ag nanoparticles homogenously dispersed in the Pt shell (the inset in Fig. 6d).

On the basis of the above-mentioned experimental results and theoretical analysis, a catalytic mechanism is proposed as illustrated in Scheme 1 (Part 2). According to the traditional theory in terms of the catalytic reduction of *p*-nitrophenol by Ag nanoparticles [38,39], electrons transfer from BH_4^- to *p*-nitrophenol through adsorption of the reactant molecules onto the catalyst surface, and the catalytic efficiency is highly dependent on the large surface areas of nanoparticle catalyst. In this regard, the high activity of the TiO_2 NW@hollow Ag/Pt heterostructures catalyst was attributed to the high surface-to-volume ratio and the accessible interfaces between Ag and Pt with different work functions. The catalytic function of Ag is lower than that of Pt. It is well-known that Fermi level alignment occurs whenever two dissimilar metals are put into contact, resulting in charge redistribution [40]. Therefore, electrons leave Ag from a thus depleted region near Pt/Ag interface into Pt, and approach an electron-enriched region. Existence of these surplus/depletion electrons inside the metals facilitates the uptake/release of electrons by molecules that happen to be close to these regions (atop the Ag/Pt hollow nanostructures). The regions with excessive electrons were increased due to more interfaces, which concomitantly increase the possibility for randomly absorbed molecules to give rise to reactions at such regions. On the other hand, the TiO_2 acted as an electron donor to activate Ag/Pt heterostructures, resulting in a higher electronic density on the Ag/Pt heterostructure surface, thus promoting the catalytic performance of the entire catalyst [41,42]. Therefore, bimetallic interfaces are expected to play as an electron relay system that opens up pathways for diverse intermediate steps in the reaction of adsorbed species. Recent studies provide insights into the improved catalytic activity of bimetal nanostructures [17,18,43]. According to the experimental results, the TiO_2 NW@hollow Ag/Pt heterostructures offere the accessible Ag/Pt interfaces, which are responsible for the high catalytic efficiency.

4. Conclusions

TiO_2 NW@hollow Ag/Pt heterostructures were synthesized by a simple solution reaction method. Results reveal that the catalytic activity of the TiO_2 NW@hollow Ag/Pt catalyst is improved due to the accessible interfaces and high surface-to-volume ratio. Meanwhile, the Ag/Pt bimetal nanostructures decorated on the TiO_2 NW enhance their stability, dispersibility, recycling and reusability. The TiO_2 NW@hollow Ag/Pt catalyst show an excellent catalytic performance to hydrogenate *p*-nitrophenol with $NaBH_4$ as a reducing agent in aqueous phase, which yields the conversion rate of *p*-nitrophenol as high as ~95% within 9 min under atmosphere and room temperature. Notably, the TiO_2 NW@hollow Ag/Pt catalyst still displays an excellent recycling and reusability even after 8 times reducing reaction of *p*-nitrophenol into *p*-aminophenol.

Acknowledgments

This work was supported by the National Natural Science Foundation of China (No. 51272235, 51436001); National High-tech R&D Program of China(2013AA031702); Program for New Century Excellent Talents in University (NCET-13-0998); Fundamental Research Funds for the Central Universities (230201406500016); Zhejiang Provincial Natural Science Foundation of China (LR12E02001).

Appendix A. Supplementary data

Supplementary data associated with this article can be found, in the online version, at http://dx.doi.org/10.1016/j.apcatb.2015.06.033

References

[1] S. Guo, X. Zhang, W. Zhu, K. He, D. Su, A. Mendoza-Garcia, S.F. Ho, G. Lu, S. Sun, J. Am. Chem. Soc. 136 (2014) 15026–15033.
[2] A.T.N. Dao, D.M. Mott, K. Higashimine, S. Maenosono, Sensors 13 (2013) 7813–7826.
[3] J. Chen, B. Wiley, J. McLellan, Y. Xiong, Z.-Y. Li, Y. Xia, Nano Lett. 5 (2005) 2058–2062.
[4] L. Chen, L. Kuai, X. Yu, W. Li, B. Geng, Chem. Eur. J. 19 (2013) 11753–11758.
[5] S. Alayoglu, A.U. Nilekar, M. Mavrikakis, B. Eichhorn, Nat. Mater. 7 (2008) 333–338.
[6] J.-M. Yan, X.-B. Zhang, T. Akita, M. Haruta, Q. Xu, J. Am. Chem. Soc. 132 (2010) 5326–5327.
[7] J. Gao, X. Ren, D. Chen, F. Tang, J. Ren, Scripta Mater. 57 (2007) 687–690.
[8] Y. Li, P. Zhou, Z. Dai, Z. Hu, P. Sun, J. Bao, New J. Chem. 30 (2006) 832–837.
[9] Z. Bai, L. Yang, J. Zhang, L. Li, J. Lv, C. Hu, J. Zhou, Catal. Commun. 11 (2010) 919–922.
[10] W. Zhang, J. Yang, X. Lu, ACS Nano 6 (2012) 7397–7405.
[11] L. Kuai, S. Wang, B. Geng, Chem. Commun. 47 (2011) 6093–6095.
[12] E.C. Cho, P.H. Camargo, Y. Xia, Adv. Mater. 22 (2010) 744–748.
[13] H. Liu, J. Qu, Y. Chen, J. Li, F. Ye, J.Y. Lee, J. Yang, J. Am. Chem. Soc. 134 (2012) 11602–11610.
[14] L.C. Jones, Z. Buras, M.J. Gordon, J. Phys. Chem. C 116 (2012) 12982–12988.
[15] L.C. Jones, M.J. Gordon, J. Phys. Chem. C 116 (2012) 23472–23476.
[16] H. Li, H. Wu, Y. Zhai, X. Xu, Y. Jin, ACS Catal. 3 (2013) 2045–2051.
[17] C. Li, Y. Yamauchi, Phys. Chem. Chem. Phys. 15 (2013) 3490–3496.
[18] J. Huang, S. Vongehr, S. Tang, H. Lu, X. Meng, J. Phys. Chem. C 114 (2010) 15005–15010.
[19] G. Chen, D. Xia, Z. Nie, Z. Wang, L. Wang, L. Zhang, J. Zhang, Chem. Mater. 19 (2007) 1840–1844.
[20] H. Li, H. Lin, Y. Hu, H. Li, P. Li, X. Zhou, J. Mater. Chem. 21 (2011) 18447–18453.
[21] W. Dong, T. Zhang, J. Epstein, L. Cooney, H. Wang, Y. Li, Y.-B. Jiang, A. Cogbill, V. Varadan, Z.R. Tian, Chem. Mater. 19 (2007) 4454–4459.
[22] M. Zhu, P. Chen, W. Ma, B. Lei, M. Liu, ACS Appl. Mater. Interfaces 4 (2012) 6386–6392.
[23] Z. Yan, G. Compagnini, D.B. Chrisey, J. Phys. Chem. C 115 (2011) 5058–5062.
[24] J. Zhao, G.P. Huffman, B.H. Davis, Catal. Lett. 24 (1994) 385–389.
[25] A.V. Vorontsov, E.N. Savinov, J.S. Zhen, J. Photochem. Photobiol. A 125 (1999) 113–117.
[26] L.K. Ono, J.R. Croy, H. Heinrich, B. Roldan Cuenya, J. Phys. Chem. C 115 (2011) 16856–16866.
[27] P. Bera, K. Priolkar, A. Gayen, P. Sarode, M. Hegde, S. Emura, R. Kumashiro, V. Jayaram, G. Subbanna, Chem. Mater (2003) 2049–2060.
[28] W. Li, L. Kuai, L. Chen, B. Geng, Sci. Rep. 3 (2013) 2377.
[29] W. Hu, B. Liu, Q. Wang, Y. Liu, P. Jing, S. Yu, L. Li, J. Zhang, Chem. Commun. 49 (2013) 7596–7598.
[30] A.A. Ismail, A. Hakki, D.W. Bahnemann, J. Mol. Catal. A-Chem. 358 (2012) 145–151.
[31] Y. Li, Y. Ding, J. Phys. Chem. C 114 (2010) 3175–3179.
[32] M. Inoue, A. Nakazawa, M. Umeda, Int. J. Hydrogen Energy 37 (2012) 1226–1235.
[33] S.-D. Oh, M.-R. Kim, S.-H. Choi, J.-H. Chun, K.-P. Lee, A. Gopalan, C.-G. Hwang, K. Sang-Ho, O.J. Hoon, J. Ind. Eng. Chem. 14 (2008) 687–692.
[34] X. Wang, D. Liu, S. Song, H. Zhang, J. Am. Chem. Soc. 135 (2013) 15864–15872.
[35] P. Pachfule, S. Kandambeth, D.D. Díaz, B. Rahul, Chem. Commun. 50 (2014) 3169–3172.
[36] H. Wang, L. Chen, Y. Feng, H. Chen, Acc. Chem. Res. 46 (2013) 1636–1646.
[37] J. Huang, S. Vongehr, S. Tang, H. Lu, J. Shen, X. Meng, Langmuir 25 (2009) 11890–11896.
[38] W. Zhang, F. Tan, W. Wang, X. Qiu, X. Qiao, J. Chen, J. Hazard. Mater. 217 (2012) 36–42.
[39] D.K. Bhui, A. Misra, Carbohydr. Polym. 89 (2012) 830–835.
[40] A. Zangwill, Physics at Surfaces, Cambridge University Press, 1988.
[41] J.L. Shi, Chem. Rev. 113 (2013) 2139–2181.
[42] D.H. Zhang, G.D. Li, J.X. Li, J.S. Chen, Chem Commun. 341 (2008) 3414–3416.
[43] N.R. Jana, Z. Wang, T. Pal, Langmuir 16 (2000) 2457–2463.